The spatiotemporal changes in dopamine, neuromelanin and iron characterizing Parkinson's disease

Emma Biondetti, Mathieu D Santin, Romain Valabrègue, Graziella Mangone, Rahul Gaurav, Nadya Pyatigorskaya, Matthew Hutchison, Lydia Yahia-Cherif, Nicolas Villain, Marie-Odile Habert, et al.

The spatiotemporal changes in dopamine, neuromelanin and iron characterizing Parkinson's disease

Emma Biondetti,[1,2,3] Mathieu D. Santin,[1,2] Romain Valabrègue,[1,2] Graziella Mangone,[1,4,5] Rahul Gaurav,[1,2,3] Nadya Pyatigorskaya,[1,3,6] Matthew Hutchison,[7] Lydia Yahia-Cherif,[1,2] Nicolas Villain,[1,5] Marie-Odile Habert,[8,9] Isabelle Arnulf,[1,3,10] Smaranda Leu-Semenescu,[10] Pauline Dodet,[10] Miquel Vila,[11] Jean-Christophe Corvol,[1,4,5] Marie Vidailhet,[1,3,5] and Stéphane Lehéricy[1,2,3,6]

Abstract

In Parkinson's disease, there is a progressive reduction in striatal dopaminergic function, and loss of neuromelanin-containing dopaminergic neurons and increased iron deposition in the substantia nigra. We tested the hypothesis of a relationship between impairment of the dopaminergic system and changes in the iron metabolism. Based on imaging data of patients with prodromal and early clinical Parkinson's disease, we assessed the spatiotemporal ordering of such changes and relationships in the sensorimotor, associative and limbic territories of the nigrostriatal system.

Patients with Parkinson's disease (disease duration < 4 years) or idiopathic REM sleep behaviour disorder (a prodromal form of Parkinson's disease) and healthy controls underwent longitudinal examination (baseline and 2-year follow-up). Neuromelanin and iron sensitive MRI and dopamine transporter single-photon emission tomography were performed to assess nigrostriatal levels of neuromelanin, iron, and dopamine. For all three functional territories of the nigrostriatal system, in the clinically most and least affected hemispheres separately, the following was performed: cross-sectional and longitudinal inter-group difference analysis of striatal dopamine and iron, and nigral neuromelanin and iron; in Parkinson's disease patients, exponential fitting analysis to assess the duration of the prodromal phase and the temporal ordering of changes in dopamine, neuromelanin or iron relative to controls; voxel-wise correlation analysis to investigate concomitant spatial changes in dopamine-iron, dopamine-neuromelanin and neuromelanin-iron in the substantia nigra pars compacta.

The temporal ordering of dopaminergic changes followed the known spatial pattern of progression involving first the sensorimotor, then the associative and limbic striatal and nigral regions. Striatal dopaminergic denervation occurred first followed by abnormal iron

metabolism and finally neuromelanin changes in the substantia nigra pars compacta, which followed the same spatial and temporal gradient observed in the striatum but shifted in time.

In conclusion, dopaminergic striatal dysfunction and cell loss in the substantia nigra pars compacta are interrelated with increased nigral iron content.

Author affiliations:

1 Sorbonne Université, Institut du Cerveau – Paris Brain Institute – ICM, INSERM, CNRS, 75013 Paris, France

2 ICM, Centre de NeuroImagerie de Recherche – CENIR, 75013 Paris, France

3 ICM, Team "Movement Investigations and Therapeutics" (MOV'IT), 75013 Paris, France

4 Assistance Publique Hôpitaux de Paris, Hôpital Pitié-Salpêtrière, Department of Neurology, Centre d'Investigation Clinique Neurosciences, 75013 Paris, France

5 Assistance Publique Hôpitaux de Paris, Hôpital Pitié-Salpêtrière, Department of Neurology, 75013 Paris, France

6 Assistance Publique Hôpitaux de Paris, Hôpital Pitié-Salpêtrière, Department of Neuroradiology, 75013 Paris, France

7 Biogen Inc., Cambridge, MA 02142, USA

8 Assistance Publique Hôpitaux de Paris, Hôpital Pitié-Salpêtrière, Department of Nuclear Medicine, 75013 Paris, France

9 Sorbonne Université, CNRS, INSERM, Laboratoire d'Imagerie Biomédicale – LIB, 75006 Paris, France

10 Assistance Publique Hôpitaux de Paris, Hôpital Pitié-Salpêtrière, Sleep Disorder Unit, 75013 Paris, France

11 Neurodegenerative Diseases Research Group, Vall d'Hebron Research Institute (VHIR)-Center for Networked Biomedical Research on Neurodegenerative Diseases (CIBERNED)-Department of Biochemistry and Molecular Biology, Autonomous University of Barcelona (UAB)-Catalan Institution for Research and Advanced Studies (ICREA), 08010 Barcelona, Spain

Correspondence to: Emma Biondetti, PhD

Institute for Advanced Biomedical Technologies, Department of Neuroscience, Imaging and Clinical Sciences, "G. D'Annunzio University" of Chieti-Pescara, Via Luigi Polacchi 11, 66100 Chieti, Italy

E-mail: emma.biondetti@unich.it

Running title: Nigrostriatal changes in parkinsonism

Introduction

Parkinson's disease is a neurological disorder characterised by progressive degeneration of dopaminergic neuromelanin-containing cells in the substantia nigra pars compacta (SNc) and reduced striatal dopaminergic function associated with increased iron deposition in the substantia nigra (SN).[1, 2] Changes occur after a long prodromal phase[1] preceding motor symptom onset by 10 to 25 years for putaminal dopamine uptake[3] and by 5 years for SNc volume loss (assessed using neuromelanin signal changes).[4] Iron levels also increase before motor sign manifestation in patients with idiopathic REM sleep behaviour disorder (iRBD), a prodromal condition of parkinsonism,[5] and in both symptomatic and asymptomatic carriers of the LRRK2 and Parkin mutations,[6] but the time to onset before motor sign appearance is unknown.

Dopamine, neuromelanin, and iron concentrations probably are tightly linked. First, they all participate in the dopamine metabolic pathway, whose end-stage product is neuromelanin. In dopaminergic neurons, neuromelanin can chelate excess iron, providing a neuroprotective role.[2, 7] However, excess intracellular neuromelanin could also compromise neuronal function and trigger Parkinson's disease-like pathology.[8] Second, previous imaging studies in Parkinson's disease have partially investigated the relationship between neuromelanin, iron, and dopamine with mixed results.[5, 9-14] Most have reported positive correlations between striatal dopamine transporter (DaT) and nigral neuromelanin levels.[9-12] Results on iron assessment are contradictory, as some studies reported negative correlations with nigral neuromelanin levels[13, 14] and striatal DaT levels.[12] Others found no correlation in Parkinson's disease between nigral iron and neuromelanin[12, 13] or between nigral iron and striatal DaT.[12] Likewise, in iRBDs, nigral iron levels assessed using transcranial sonography did not correlate with striatal DaT, suggesting independency of dopaminergic dysfunction and iron increase.[5] Third, the progression of changes is spatially specific, starting in sensorimotor areas of the striatum and the SN.[9, 15] SN iron accumulation may also follow a spatial gradient of degeneration,[14, 16] although not all studies agree.[13] Additionally, nigral changes differed between the neuromelanin-rich SNc, where disease-related iron accumulation is expected, and the naturally iron-rich SN pars reticulata.[17] Most studies did not specifically investigate where neurodegeneration occurred nor investigated prodromal Parkinson's disease.[12, 13] A relationship between changes in these three compounds should translate into spatiotemporal relationships between their changes, observable in each functional territory of the basal ganglia.

Here, we aimed to investigate the relationship between dopaminergic dysfunction and changes in neuromelanin and iron concentrations in the nigrostriatal system in patients with prodromal and clinical Parkinson's disease. Particularly, we aimed to assess the temporal ordering of such changes and their spatial distribution within the nigrostriatal system's sensorimotor, associative, and limbic territories.

Materials and methods

Participants

The ICEBERG longitudinal cohort was prospectively investigated.[4] This cohort included healthy control subjects (HCs), iRBD patients and Parkinson's disease patients assessed at baseline (V1) and after 2 years (V2). Patient inclusion criteria comprised a clinical diagnosis of iRBD or Parkinson's disease, respectively performed by sleep neurologists and movement disorder specialists, 18–75 years of age, minimal or no cognitive disturbances (Mini-Mental State Examination score > 26/30) and, for Parkinson's disease patients, time elapsed from the first appearance of motor symptoms (i.e., disease duration) < 4 years. Patients with Parkinson's disease met the UK Parkinson's disease Society Brain Bank criteria.[18] Patients with iRBD had a history of dream-enacting behaviours with (potentially) injurious movements and enhanced tonic chin muscle tone or complex behaviours during REM sleep but did not meet the criteria for Parkinson's disease or dementia.[19] The local ethics committee approved this study (RCB: 2014-A00725-42) and all participants gave written informed consent.

Clinical examination

Clinical examination included the Hoehn and Yahr scale, which evaluates the severity of Parkinson's disease-related symptoms;[20] the Movement Disorder Society Unified Parkinson's Disease Rating Scale (MDS-UPDRS)[21] part III in the OFF condition,[21] which evaluates motor disability >12 hours after withdrawing dopaminergic treatment; the Mattis dementia rating scale (DRS)[22, 23] and the Montréal cognitive assessment score (MoCA),[24] which evaluate cognitive impairment; and Ardouin's scale of behaviour in Parkinson's disease (ASBPD),[25, 26] which evaluates mood/behavioural status. In Parkinson's disease patients, the body side of first motor symptoms was defined as the clinically most affected.

Imaging data acquisition

All subjects underwent MRI on a Siemens Prisma 3 T system (Siemens Healthcare, Erlangen, Germany) using a 64-channel head coil for signal reception. The following images were acquired: whole-brain T_1-weighted 3D MP2RAGE (three-dimensional magnetisation-prepared two rapid gradient echo) for anatomical reference;[27] T_1-weighted 2D TSE (two-

dimensional turbo spin echo) with a field of view restricted to the midbrain for neuromelanin-sensitive imaging;[28] and whole-brain T_2*-weighted multi-echo 3D FLASH (fast low angle shot) for iron-sensitive quantitative susceptibility mapping (QSM).[29] Supplementary Table 1 lists all the parameters for the MRI acquisition. The MR images were visually inspected, and those with severe motion, arterial flow artifacts affecting SN visibility or incomplete SN coverage were excluded.

In a subset of participants, DaT single-photon emission tomography imaging was performed on a hybrid gamma camera Discovery 670 Pro system (GE Healthcare, Chicago, IL) using the ^{123}I-FP-CIT tracer (DaTScan™). All subjects received thyroid gland blockade via one dose of Lugol regimen and an intravenous injection of ^{123}I-FP-CIT tracer (185-200 MBq) and underwent DaTScan™ between 3 and 4 hours after tracer injection. The acquisition parameters were circular orbit, clockwise rotation, zoom factor = 1.5\1.5, matrix size = 128x128 voxels, number of slices = 128, voxel size = 2.9x2.9 mm^2, slice thickness = 2.9 mm, rotations = 1, number of frames in rotation = 120, actual frame duration = 30 s, energy window = 143.1–174.9 KeV. All DaTScan™ images were reconstructed on the GE Healthcare Xeleris Workstation using an iterative algorithm followed by spatial filtering (fourth-order low-pass filter with a cut-off frequency equal to 3.5 mm^{-1}) and Chang attenuation correction ($\mu = 0.12$ cm^{-1}).[30]

Image analysis

When not otherwise stated, all analyses were carried out using MATLAB (R2017b, The MathWorks, Natick, MA, USA).

For QSM calculation in each subject, the gradient echo signal magnitude and phase from multiple channels of the receive coil were combined using an in-house optimised method.[31] Then, the local field map was calculated by nonlinear fitting the complex gradient echo signal over echo times,[32] background magnetic fields were removed using the Laplacian boundary value method[33] and the local field-to-magnetic susceptibility inverse problem was solved using the L1-Morphology Enabled Dipole Inversion method.[32, 34-36] Each QSM image was referenced by subtracting the average QSM value measured in the posterior limb of the internal capsule, a region characterised by stable magnetic susceptibility values.[37] The posterior limb of the internal capsule was delineated by aligning the Eve magnetic susceptibility template[38] to the subject's QSM image via the corresponding magnitude image.

Each subject's QSM and neuromelanin-sensitive images were aligned to an ad-hoc symmetric brain template, enabling analysis in a common anatomical space.[4] Particularly, each QSM or neuromelanin-sensitive image was first rigidly aligned to the T_1-weighted anatomical image.[39] Then, the T_1-weighted anatomical image was aligned to the template by concatenating an affine and a non-rigid registration.[40] Then, the same spatial transformation from the T_1-weighted image to template was applied to the neuromelanin-sensitive and QSM images.[39, 40] To mitigate the negative effect on the statistical analysis of both potential spatial misregistration and data dispersion in multiple voxel-wise tests, before quantitative analysis all coregistered images were spatially smoothed via convolution with a 1-mm wide 3D Gaussian kernel. This modest kernel width was chosen to enhance the detection of small-scale effects in the SN, while mitigating partial volume effects with the neighbouring cerebrospinal fluid.

In template space, signal-to-noise ratios (SNRs) of neuromelanin-sensitive MRI were calculated relative to a background region of interest (ROI) including the tegmentum and superior cerebellar peduncles similar to a previous study.[4]

In each subject, striatal DaT specific binding ratios (SBRs) were calculated as follows. The DaTScan™ image was rigidly aligned to the corresponding T_1-weighted anatomical MRI via the corresponding computed tomography image. Partial volume artifacts were corrected using Yang's iterative method (seven iterations) as follows.[41] Based on structural segmentations of the T_1-weigthed image calculated using FSL FIRST,[42, 43] five masks were calculated corresponding to five tissue compartments (white matter, cerebrospinal fluid, and three grey matter compartments). These compartments were defined according to their dopaminergic density level, as measured post-mortem in humans.[44] Particularly, the three grey matter compartments respectively included regions with high (nucleus accumbens, caudate nucleus, and putamen), intermediate (globus pallidus) and low dopaminergic density levels (thalamus and cortex). To normalise the signal intensity of the DaTScan™ image, thus obtaining SBR values, a reference ROI was defined in the occipital lobe by non-linearly aligning the automated anatomical labelling template[45] to the T_1-weighted anatomical image. The partial volume corrected DaTScan™ image was referenced to the average signal intensity in this occipital ROI.[46]

For each subject, in the striatum, the sensorimotor, associative and limbic putamen, the sensorimotor, associative and limbic caudate nucleus, and the nucleus accumbens were

automatically segmented by aligning a digital template of the human basal ganglia (YeB atlas)[47, 48] to the subject's anatomical T_1-weighted MRI. In each striatal ROI, the average DaT-SBR and iron sensitive QSM signal were calculated. In the midbrain, an ROI mostly corresponding to the SNc was used, which was previously calculated in template space based on neuromelanin-sensitive MRI of sixty-one HCs.[4] Further, this SNc ROI was manually segmented based on the functional subdivision of the SN in primates obtaining three subregions: dorsolateral sensorimotor, dorsomedial associative and ventral limbic.[49] In each nigral subregion, both the voxel-wise and average values of the QSM signal and the neuromelanin SNR were calculated.

Before template alignment, the MR images and DaT-SBR values of Parkinson's disease patients were lateralised so that the clinically most affected side was aligned with the left hemisphere. In iRBD, there is no "most affected side", thus here, to perform lateralisation, the brain hemisphere with the lowest mean of global striatal DaT-SBR was selected as the potential side of future appearance of Parkinson's disease-related motor symptom. HC data were not lateralised.

For each patient and each striatal region, the DaT-SBR percent ratio (%) was calculated as the ratio of the patient's DaT-SBR to the average DaT-SBR in HCs. Similarly, the QSM and neuromelanin SNR percent ratios were calculated in each SN subregion.

For each striatal region, the DaT-SBR percent ratio of individual Parkinson's disease patients was modelled against disease duration using an exponential fitting curve as, in Parkinson's disease, degeneration of the nigrostriatal system has been shown to occur at a faster rate in the early phases of disease than in later phases.[1, 3, 4, 15] Based on the exponential fitting curve, the prodromal phase of disease and the DaT-SBR loss at the time of diagnosis were respectively calculated as the time closest to $t = 0$ where DaT-SBR = 100%, and the zero-intercept of the curve. Based on inverse mapping of the exponential fitting, the temporal placement of the average DaT-SBR ratio in iRBDs at V1 was estimated. Similar to striatal DaT-SBR, for each SN subregion, the QSM and neuromelanin SNR percent ratios of individual Parkinson's disease patients over disease duration were modelled using exponential fitting functions. Then, the prodromal phase of disease and the variation in QSM signal or neuromelanin SNR at the time of disease diagnosis were calculated.

Statistical analysis

Statistical analyses were performed using MATLAB and R (v3.6.1).[50] All statistical tests were two-tailed and $P < 0.05$ was considered to determine significance.

At V1, adjusted between-group differences in age and clinical scores were estimated using ANOVA and Tukey's post-hoc test for all-pairwise comparisons. Adjusted sex differences were estimated using Pearson's chi-square test with Yates' continuity correction and the false discovery rate procedure.

In all the following analyses, sex and age were included as covariates of no interest. Indeed, both sex and age influence the phenotypical expression of Parkinson's disease,[51] healthy aging induces neuromelanin and iron accumulation in the nigrostriatal system[52-54] and DaT decrease in the striatum,[55] and sex influences both DaT uptake and neuromelanin accumulation with healthy aging.[54, 56]

For each ROI, visit and hemisphere, inter-group differences in DaT, iron and neuromelanin were estimated using linear models plus Tukey's post-hoc test, with the imaging-based measurement (the average DaT-SBR, neuromelanin SNR or QSM) as the continuous dependent variable, group and sex as categorical variables and age as a linear effect. Similarly, for each ROI and hemisphere, inter-visit differences in DaT, iron and neuromelanin were estimated using linear models plus Tukey's post-hoc test, with the inter-visit difference of the imaging-based measurement as the continuous dependent variable and the inter-visit time as a linear effect.

To evaluate spatially specific concomitant changes between striatal DaT and nigral neuromelanin or iron, Pearson's correlations were calculated between the average DaT-SBR in each striatal ROI and the voxel-wise values of nigral neuromelanin SNR or QSM in the SNc, simultaneously adjusting for multi-voxel (SNc) and multi-ROI (striatum) comparisons using an approximate multivariate permutation method.[57] Similarly, to estimate spatially specific concomitant changes in nigral neuromelanin and iron, voxel-wise Pearson's correlations were calculated between neuromelanin SNR and QSM in the SNc, adjusting for multi-voxel comparisons using the false discovery rate procedure. For all correlation analyses, baseline data from iRBD patients and Parkinson's disease patients were considered to explore changes along a pseudo-temporal axis of disease, but V2 data were excluded to avoid introducing intra-subject correlation bias.

Data availability

The data supporting the findings of this study are available from the corresponding author upon reasonable request.

Results

Demographic and clinical characteristics

Patient characteristics are summarised in Table 1. Between May 2015 and September 2019, 55 HCs, 43 patients with iRBD, and 135 patients with idiopathic Parkinson's disease were enrolled and underwent MRI at V1. Monogenic cases of Parkinson's disease were not included in this study. A subset of these subjects underwent MRI at V2, and DaTScan™ at V1 and V2 (Table 1). All subjects underwent MRI on the clinical assessment day and DaTScan™ within 6 months of MRI. Only four iRBDs returned within 3 months after clinical assessment due to unavailability of the MRI scanner. No subjects were entirely excluded following MRI quality control, as they all contributed at least one measurement to the analysis (Supplementary Material).

At V1, iRBD patients were older than both HCs ($P = 0.004$) and Parkinson's disease patients ($P < 0.001$). The male/female ratio was higher among iRBD patients compared to both HCs ($P = 0.002$) and Parkinson's disease patients ($P = 0.005$). The three groups differed in Hoehn and Yahr stage (all $P < 0.001$) and MDS-UPDRS-III OFF score (all $P < 0.001$). All groups had similar MoCA scores, whereas iRBD patients had a lower Mattis DRS score than HCs ($P = 0.04$). Parkinson's disease patients had higher hypodopaminergic ASBPD than HCs, and higher hyperdopaminergic ASBPD scores than both HCs and iRBD patients (all $P < 0.001$). Dopaminergic medication was administered to 121 Parkinson's disease patients at V1, and to 4 iRBD patients and 77 Parkinson's disease patients at V2.

Group differences in DaT, neuromelanin and iron

At V1, Parkinson's disease patients had lower DaT levels than HCs and iRBD patients in all striatal regions bilaterally (Figs. 1B and 1C). In the clinically most affected hemisphere, all territories of the caudate nucleus and putamen were similarly affected, whereas the limbic

striatum was less affected (Fig. 1B). In the contralateral hemisphere, the putamen was the most affected with all territories similarly involved, followed by the caudate nucleus and the nucleus accumbens (Figs. 1E and 1F). In the caudate nucleus, sensorimotor subregions were more affected, followed, in order, by the associative and the limbic subregions for both Parkinson's disease patients compared to HCs (Figs. 1B and 1E) and Parkinson's disease patients compared to iRBD patients (Figs. 1C and 1F). In iRBD patients compared to HCs, DaT loss was significant in the sensorimotor putamen bilaterally and, less, in the associative putamen in the most affected hemisphere (Figs. 1D and 1G). In Parkinson's disease patients at V2, a similar pattern was observed bilaterally (Figs. 1H and 1K). At V2, DaT loss in iRBD patients compared to HCs progressed in all striatal subregions except the bilateral nucleus accumbens (Fig. 1J) and the caudate nucleus in the least affected hemisphere (Fig. 1M). However, in the most affected hemisphere, inter-visit DaT loss was only significant in the sensorimotor and the associative putamen (Fig. 1P). In the least affected hemisphere, inter-visit DaT loss was only significant in the associative caudate nucleus of Parkinson's disease patients compared to HCs (Fig. 1Q). Overall, similar spatial gradients were found bilaterally, with increased severity in the most affected hemisphere. Conversely, no striatal region exhibited inter-group differences in iron.

In the most affected hemisphere at V1, neuromelanin loss was significant in the whole SNc of Parkinson's disease patients compared to both HCs and iRBD patients (Figs. 2B and 2C). At V2, neuromelanin loss was significant in the whole SNc of Parkinson's disease patients compared to HCs (Fig. 2F) and in the sensorimotor SNc of Parkinson's disease patients compared to iRBD patients (Fig. 2G). In the least affected hemisphere, at V1 there were no changes. At V2, neuromelanin loss was significant in the sensorimotor and associative SNc of Parkinson's disease patients compared to HCs (Fig. 2H) and in the sensorimotor SNc of iRBD patients compared to HCs (Fig. 2I). Overall, neuromelanin changes followed the expected gradient: the dorsolateral sensorimotor SNc was more impacted in Parkinson's disease patients in the most affected hemisphere at V1 (Fig. 2B) and the least affected hemisphere at V2 (Fig. 2H) and in iRBD patients in the least affected hemisphere at V2 (Fig. 2I). Iron accumulation was only significant in the whole SNc of Parkinson's disease patients compared to HCs without gradients in the most affected hemisphere at V1 (Fig. 2B) and in the associative SNc of Parkinson's disease patients compared to HCs in the least affected hemisphere at V2 (Fig. 2H). There were no inter-visit group differences in neuromelanin or iron in the bilateral SNc. Similar to the striatum, SNc degeneration appeared to start in the

clinically most affected hemisphere and to similarly (but less severely) progress contralaterally.

Scatter boxplots of DaT-SBR measurements in the striatum and neuromelanin SNR and QSM measurements in the SNc are shown in Supplementary Figs. 1-13.

Temporal progression of global changes in DaT, neuromelanin and iron

Similar to the spatial group differences, DaT loss in Parkinson's disease patients progressively involved the sensorimotor, associative and limbic putamen, the sensorimotor, associative and limbic caudate nucleus, and the nucleus accumbens bilaterally (Fig. 3, Supplementary Table 3). The estimated prodromal phase of DaT loss lasted between 20.7 years (sensorimotor putamen) and 1.1 years (nucleus accumbens) (Supplementary Table 3). At V1, estimated DaT losses in iRBD patients were comparable to those in Parkinson's disease patients 16.5 years before disease diagnosis (sensorimotor putamen), whereas values in the nucleus accumbens were within normal ranges (Supplementary Table 3).

In the most affected hemisphere of Parkinson's disease patients, estimated SNc iron accumulation started 9.6 years (sensorimotor), 6.2 years (associative) or 4.1 years (limbic) before diagnosis, whereas estimated neuromelanin loss started 5.9 years (sensorimotor) or 3.6 years (associative) before diagnosis (Fig. 3). In both the limbic and the whole SNc in the least affected hemisphere, neuromelanin signal changes were minimal.

Spatiotemporal DaT-neuromelanin-iron correlation patterns

In the most affected hemisphere, DaT-neuromelanin (Figs. 4A-G), neuromelanin-iron (Fig. 4K) and DaT-iron (Figs. 4L-R) correlated significantly in the SNc. Both the neuromelanin-DaT and iron-DaT correlation patterns appeared as longitudinal bands extending through the SNc full anteroposterior length and occupying large fractions of the SNc width (Figs. 4A-G and 4L-R). In the SNc, the neuromelanin-DaT correlation patterns of all putaminal territories overlapped considerably (Fig. 4H). In the most affected hemisphere, neuromelanin-DaT correlations always extended over a larger SNc area than in the least affected hemisphere (Figs. 4A-G). Despite the considerable overlap in the SNc, the territories of the caudate nucleus exhibited an anterolateral-to-posteromedial gradient extending from the sensorimotor to the limbic caudate nucleus with the associative caudate nucleus in between (Fig. 4I).

Similar gradients were found for the limbic putamen (anterolateral), the limbic caudate nucleus (intermediate) and the nucleus accumbens (posteromedial) (Fig. 4J). The iron-DaT correlations considerably overlapped for all striatal regions (Figs. 4L-R). Unlike the neuromelanin-DaT correlations, the iron-DaT correlations involved the bilateral SNc for all striatal regions except the nucleus accumbens (Figs. 4L-R). In patients, neuromelanin-iron correlations appeared in the bilateral anterior SNc, corresponding to associative and limbic areas (Fig. 4K).

Discussion

This study reveals that changes in neuromelanin and iron in the SNc and DaT in the striatum followed similar spatial and time-shifted temporal patterns along the sensorimotor, associative and limbic territories. First, synaptic dopaminergic dysfunction occurred in the striatum, then iron changes and neuromelanin loss occurred in the SNc. Changes correlated in the SNc. These results suggest an interrelationship between dopaminergic striatal dysfunction, nigral cell loss and increased nigral iron content.

Topography of changes

Parkinson's disease patients exhibited the expected gradient of DaT loss, progressively involving the sensorimotor, anterodorsal associative and limbic ventral striatal regions,[58] and greater neuromelanin loss in the posterolateral sensorimotor SNc than in the anteromedial associative and limbic SNc.[4] Nigral iron was evenly increased in the SNc, as previously reported using iron-sensitive MRI in Parkinson's disease,[59, 60] but unlike previous findings suggesting higher iron in the lateral SN.[13] A recent meta-analysis showed greater iron increase in the lateral SNc than in the medial SNc when using iron-sensitive R_2* measurements but not when using QSM.[60] Others found that QSM changes spanned larger areas of the bilateral SNc than R_2* changes,[61] or were restricted to ventral SN regions not isolated here.[16] Thus, spatial gradients of iron deposition need further investigation.

In iRBD patients, striatal DaT loss exhibited the same spatial gradient but with a lower magnitude than in Parkinson's disease patients, consistent with observations in larger striatal areas.[5] Moreover, the presence of significant DaT loss without significant neuromelanin loss

reflected the known earlier degeneration of striatal terminals in Parkinson's disease.[62] Patients with iRBD had no significant changes in nigral neuromelanin SNR at V1,[4] but only in the sensorimotor SNc at V2.[4] Similarly, iRBD patients had no significant nigral iron changes as in a study using R_2*,[63] but in contrast with another study using QSM (which measured iron in the whole SN).[64] Inter-visit changes in neuromelanin and iron accumulation were not significant. On neuromelanin-sensitive MRI, neuromelanin SNR was less sensitive than SNc volume measurements (as used here) for detecting changes early in the disease,[65] suggesting that, in early Parkinson's disease, measurements of neuromelanin residual volume and SNc neuromelanin SNR offer complementary information on Parkinson's disease-induced temporal changes in neuromelanin.

At baseline, in the clinically least affected hemisphere, Parkinson's disease patients presented no significant neuromelanin loss or iron accumulation in the SNc. Given that the disease is probably present bilaterally by the time it manifests unilaterally, these results could have a biological explanation. After dopaminergic neuron death, neuromelanin granules can remain in the extracellular space for long periods of time due to their insolubility,[66] as has been observed in patients with Parkinson's disease,[67] normally ageing subjects,[68] and in the first rodent model of age-dependent human-like neuromelanin production in the SNc.[69] Thus, extracellular neuromelanin could still be MRI-visible for some time after neuron death, before it is phagocytised. As neuromelanin loss and iron accumulation in the SNc are tightly linked, the delayed degradation of extracellular neuromelanin could also explain the delayed observation of iron accumulation on iron-sensitive MRI. Alternatively, we cannot rule out that the MRI methods employed in the present study might have insufficient sensitivity to detect smaller-scale changes at this stage of the disease (for further discussion on methodological limitations, please refer to the "Limitations and considerations").

Temporal ordering of changes

In the most affected hemisphere, striatal dopaminergic dysfunction was estimated to start decades before disease diagnosis depending on the striatal territory: longer in the sensorimotor putamen (-20.7 years) than in the associative striatum (-12.7 to -4.4 years) and shorter in the limbic striatum (-6.1 to -1.1 years). Previous PET studies reported a 6–17-year prodromal range in the entire most affected putamen.[3] In our cohort, the estimated prodromal phase in the most affected putamen lasted 13 years, as for methylphenidate PET tracers.[3]

In the most affected hemisphere, nigral iron accumulation preceded neuromelanin loss by 2–3 years in the sensorimotor and associative territories. In the limbic SNc, the prodromal phase appeared longer, probably because of imprecise estimations due to minimal neuromelanin changes in this region. For neuromelanin loss, the average onset of the prodromal phase in the sensorimotor and associative SNc (4.8 years) agreed with our previous study (5.3 years).[4]

Spatial relationships between dopaminergic and iron changes

DaT loss in all striatal areas correlated with both SNc neuromelanin loss and iron accumulation. In the most affected hemisphere, the significant DaT-neuromelanin correlation was congruent with previous findings in Parkinson's disease,[9-12] using dopaminergic tracers in the whole striatum,[10, 11] in the whole caudate nucleus and putamen,[12] between specific striatal and nigral territories[9] and between striatal DaT and post-mortem SNc cell counts.[70] Conversely, DaT and neuromelanin were uncorrelated in more advanced Parkinson's disease, suggesting that DaTScan™ is linearly related to nigral cell losses up to 50%.[71] In the SNc, DaT loss correlated with neuromelanin loss in large overlapping areas particularly for the putamen. However, correlations with regions of the caudate nucleus from limbic to associative to sensorimotor progressively extended further posteriorly and medially in the SNc. The limbic putamen, limbic caudate nucleus and nucleus accumbens exhibited the same rostrolateral-to-caudomedial pattern. Thus, the shape and location of the DaT-neuromelanin correlation patterns partially reflected the functional organisation of striatonigral projections reported in non-human primates, although with a larger overlap,[49] potentially caused by: greater overlap in humans than in primates; loss of neuronal specificity as reported in Parkinson's disease;[72] or technical issues deriving from the coarser resolution of DaTScan™ and neuromelanin-sensitive MRI compared with histological methods. In the SNc, DaT-neuromelanin correlations were mainly lateralised in the most affected hemisphere, as previously shown.[9-11] Probably, the least affected hemisphere was progressively affected along the same time-shifted spatial gradient as the most affected hemisphere. Alternatively, this marked lateralisation could indicate different trajectories of dopaminergic neuron dysfunction and neuromelanin-containing neuron loss in early disease stages.[9]

Striatal DaT loss and nigral iron accumulation correlated in the bilateral SNc contradicting previous negative results,[12] potentially because of different nigral ROI delineations (SNc here as opposed to the entire SN in previous studies); the larger sample size examined here; or different mean disease durations (1.5 years here as opposed to 6 years in previous studies).[12]

Lastly, neuromelanin and iron only correlated in the anteromedial SNc as shown recently,[14] suggesting a correspondence of this SNc region with nigrosome-2. Contrary to previous findings, we could not identify a second cluster corresponding to nigrosome-1.[14] As nigrosome-1 is affected earlier in Parkinson's disease, possibly, neuromelanin loss and iron accumulation in this region followed different trajectories in our patient cohorts compared with the one investigated by Langley et al.[14]

The specific relationship between changes in SNc iron and those in the nigrostriatal dopaminergic pathway, spatiotemporally consistent (same temporal pattern in the three nigrostriatal territories starting with striatal dopaminergic dysfunction, followed by SNc iron accumulation preceding SNc neuromelanin loss and, hence, dopaminergic cell loss) suggested interdependent dopaminergic and iron changes. This suggests that DaT changes occurred first without dopaminergic neuron loss, congruent with recent findings in a Parkinson's disease animal model.[69] Iron deposition was not detected in early prodromal Parkinson's disease or in Parkinson's disease at V2 but was estimated to occur before the onset of neuromelanin changes. Possible explanations include insufficient QSM sensitivity for detecting small increases in iron or a non-linear iron accumulation over time. Moreover, iron and neuromelanin correlated in the anterior but not the posterolateral SNc, which had greater neuromelanin loss. Possibly, the significant DaT-iron loss reflected different aspects of Parkinson's disease progression.[2] In the anteromedial SNc with no or minimal neuromelanin loss, significant neuromelanin-iron correlations could reflect a redox-active iron overload in neuromelanin organelles preceding neuronal death.[2] In the posterolateral SNc with greater neuromelanin loss, absent neuromelanin-iron correlations could additionally reflect activated microglia and perivascular macrophage contents.[2]

Limitations and considerations

Patients with iRBD had a relatively high MDS-UPDRS-III OFF score (i.e., 11.5 ± 6.3, see Table 1). This aspect, as already discussed in a previous study on the ICEBERG cohort,[4] could result from most patients being close to phenoconversion. Approaching phenoconversion was also suggested by the fact that four iRBDs had started receiving dopaminergic medication by the time of V2 (see Table 1). In the presence of phenoconversion, previous studies on iRBD have reported relatively high MDS-UPDRS-III scores[73] (i.e., 44) and shown a faster progression of motor examination signs 1-2 years before phenoconversion.[74] Moreover, a study stratifying iRBD patients based on the outcome of

DaTScan[TM] has reported that, iRBD with or without dopaminergic denervation, had MDS-UPDRS-III scores respectively equal to 10.5 ± 7.5 (indicative of prodromal Parkinson's disease) and 6.0 ± 4.8, whereas in HCs had a score equal to 3.2 ± 3.2.[75]

The present study had a methodological limitation, as reverse extrapolating DaT-SBR values in the iRBD group based on the exponential fitting performed in the Parkinson's disease group assumed that iRBDs had a similar temporal trajectory as Parkinson's disease patients although this assumption may not apply across all individuals of either cohort. Moreover, this assumption has limited accuracy as some iRBD patients appear to have normal striatal dopaminergic function on DaT-SPECT[5, 76] or ^{18}F-DOPA PET.[77, 78] Thus, the results of reverse extrapolation should be interpreted with caution as they reflect a potentially heterogeneous iRBD group, as also suggested by the larger standard deviations in the DaT-SBR scatter boxplots in this group compared to the Parkinson's disease group (Supplementary Figs. 1-7).

There were also some technical limitations in the present study. First, the sensitivity of the imaging methods employed here, namely, 3 T MRI and DaTScan[TM], intrinsically limited the maximum spatial resolution achievable and, in turn, the accuracy of spatiotemporal variations in dopamine, neuromelanin and iron that could be detected. Based on the results of the present study, DaTScan[TM] had a higher sensitivity in detecting earlier and more subtle denervation changes in the striatum than neuromelanin-sensitive or iron-sensitive 3 T MRI in the SNc. However, it is possible that more subtle spatiotemporal variations in nigral iron or neuromelanin could be detected by performing MRI at higher field strengths (e.g., 7 T). MRI at 7 T could outperform MRI at 3 T, because of both the known shortening of tissue relaxation times and higher image resolution achievable by increasing the static magnetic field which, combined, could help detect more subtle changes in the SNc. Alternatively, increased sensitivity to neuromelanin changes in the SNc could be achieved using [18F]AV-1451 PET instead of neuromelanin-sensitive MRI.[79] Finally, even higher sensitivity to striatal changes could be attained by using PET with DaT tracers instead of DaTScan[TM] because of the higher spatial resolution achievable with PET. However, both 7 T MRI and PET are technically more challenging to employ because of the stronger magnetic field inhomogeneities induced in the brain at higher fields (MRI) or because a cyclotron is needed to produce the radiotracer on site (PET).

A second technical limitation was represented by the DaTScan^{TM} measurements, which, in addition to being sensitive to striatal dopaminergic uptake, could also reflect changes in pharmacological compensation mechanisms occurring in Parkinson's disease, such as downregulation of DaT, especially in the early phases of disease.[80] Thus, further large scale longitudinal studies using different tracers to monitor striatal pre-synaptic dopamine function (e.g., PET with VMAT2, DaT or ^{18}F-fluorodopa) and MRI are needed to assess the potentially varying spatiotemporal relationship between dopamine function, neuromelanin loss and iron deposition in the nigrostriatal system.

In general, further studies are needed to indicate which imaging-based biomarker or combination of biomarkers could provide comprehensive information on longitudinal changes in the nigrostriatal system linked to Parkinson's disease. In particular, longitudinal data spanning longer periods of time could enable updating the curves described in Fig. 3 to reflect potential plateaus in striatal DaT loss and nigral iron accumulation or neuromelanin loss. Notably, the cohort investigated here was enrolled in a prospective 5-year longitudinal study with imaging data collected at three time points (year 1, year 3, and year 5). Only data from the first two time points were considered in the present study, as data collection is ongoing. Thus, future work will involve updating the present analyses by also incorporating data from year 5.

In conclusion, the temporal evolution of changes in the nigrostriatal dopaminergic system was characterised, which progressed following the known spatial pattern from sensorimotor to associative and limbic striatal regions. Striatal dopaminergic dysfunction evaluated using DaTScan^{TM} occurred first, subsequently associated with abnormal iron metabolism and finally with a reduction in nigral neuromelanin both assessed using MRI. Neuromelanin changes followed the same (time-shifted) spatiotemporal gradient as in the striatum. Correlations between the three measures in the SNc suggested a relationship between dopaminergic changes and iron deposition in Parkinson's disease.

Acknowledgements

Funding

Competing interests

Emma Biondetti reports grants from France Parkinson and Biogen Inc during the conduct of the study.

Rahul Gaurav and Stéphane Lehéricy received grant funding from Biogen Inc.

Matthew Hutchison is an employee of and owns stock/stock options in Biogen Inc.

Nicolas Villain reports grants from Fondation Recherche Alzheimer, grants from Département Médical Universitaire APHP. Sorbonne Université, non-financial support from GE HEALTHCARE SAS, non-financial support from MERZ PHARMA France, non-financial support from UCB Pharma SA, non-financial support from MEDTRONIC France S.A.S, non-financial support from Laboratoire AGUETTANT, outside the submitted work.

Marie-Odile Habert reports receiving fees as a speaker from Lilly and as a consultant from Blue Earth company.

Isabelle Arnulf received honoraria from Roche Pharma, Idorsia Pharma and Ono Pharma, and speaking engagement from UCB Pharma, unrelated to this study.

Jean-Christophe Corvol has served in advisory boards for Air Liquide, Biogen Inc., Denali, Ever Pharma, Idorsia, Prevail Therapeutic, Theranexus, UCB; has received grants from Sanofi and the Michael J Fox Foundation.

Mathieu D. Santin, Romain Valabrègue, Graziella Mangone, Nadya Pyatigorskaya, Lydia Yahia-Cherif, Smaranda Leu-Semenescu, Pauline Dodet, Miquel Vila and Marie Vidailhet have nothing to disclose.

Supplementary material

Supplementary material is available at *Brain* online.

References

1.	Greffard S, Verny M, Bonnet AM, et al. Motor score of the Unified Parkinson Disease Rating Scale as a good predictor of Lewy body-associated neuronal loss in the substantia nigra. *Arch Neurol*. Apr 2006;63(4):584-8. doi:10.1001/archneur.63.4.584

2.	Zucca FA, Segura-Aguilar J, Ferrari E, et al. Interactions of iron, dopamine and neuromelanin pathways in brain aging and Parkinson's disease. *Prog Neurobiol*. Aug 2017;155:96-119. doi:10.1016/j.pneurobio.2015.09.012

3.	de la Fuente-Fernández R, Schulzer M, Kuramoto L, et al. Age-specific progression of nigrostriatal dysfunction in Parkinson's disease. *Ann Neurol*. May 2011;69(5):803-10. doi:10.1002/ana.22284

4.	Biondetti E, Gaurav R, Yahia-Cherif L, et al. Spatiotemporal changes in substantia nigra neuromelanin content in Parkinson's disease. *Brain*. Aug 28 2020;doi:10.1093/brain/awaa216

5.	Iranzo A, Lomeña F, Stockner H, et al. Decreased striatal dopamine transporter uptake and substantia nigra hyperechogenicity as risk markers of synucleinopathy in patients with idiopathic rapid-eye-movement sleep behaviour disorder: a prospective study. *The Lancet Neurology*. 2010;9(11):1070-1077. doi:10.1016/s1474-4422(10)70216-7

6.	Pyatigorskaya N, Sharman M, Corvol JC, et al. High nigral iron deposition in LRRK2 and Parkin mutation carriers using R2* relaxometry. *Mov Disord*. Jul 2015;30(8):1077-84. doi:10.1002/mds.26218

7.	Hare DJ, Double KL. Iron and dopamine: a toxic couple. *Brain*. Apr 2016;139(Pt 4):1026-35. doi:10.1093/brain/aww022

8.	Vila M. Neuromelanin, aging, and neuronal vulnerability in Parkinson's disease. *Mov Disord*. Oct 2019;34(10):1440-1451. doi:10.1002/mds.27776

9.   Martin-Bastida A, Lao-Kaim NP, Roussakis AA, et al. Relationship between neuromelanin and dopamine terminals within the Parkinson's nigrostriatal system. *Brain*. Jul 1 2019;142(7):2023-2036. doi:10.1093/brain/awz120

10.   Kuya K, Shinohara Y, Miyoshi F, Fujii S, Tanabe Y, Ogawa T. Correlation between neuromelanin-sensitive MR imaging and (123)I-FP-CIT SPECT in patients with parkinsonism. *Neuroradiology*. Apr 2016;58(4):351-6. doi:10.1007/s00234-016-1644-7

11.   Kuya K, Ogawa T, Shinohara Y, et al. Evaluation of Parkinson's disease by neuromelanin-sensitive magnetic resonance imaging and (123)I-FP-CIT SPECT. *Acta Radiol*. May 2018;59(5):593-598. doi:10.1177/0284185117722812

12.   Isaias IU, Trujillo P, Summers P, et al. Neuromelanin Imaging and Dopaminergic Loss in Parkinson's Disease. *Front Aging Neurosci*. 2016;8:196. doi:10.3389/fnagi.2016.00196

13.   Reimao S, Ferreira S, Nunes RG, et al. Magnetic resonance correlation of iron content with neuromelanin in the substantia nigra of early-stage Parkinson's disease. *Eur J Neurol*. Feb 2016;23(2):368-74. doi:10.1111/ene.12838

14.   Langley J, Huddleston DE, Crosson B, Song DD, Factor SA, Hu X. Multimodal assessment of nigrosomal degeneration in Parkinson's disease. *Parkinsonism Relat Disord*. Sep 16 2020;80:102-107. doi:10.1016/j.parkreldis.2020.09.021

15.   Nandhagopal R, Kuramoto L, Schulzer M, et al. Longitudinal progression of sporadic Parkinson's disease: a multi-tracer positron emission tomography study. *Brain*. Nov 2009;132(Pt 11):2970-9. doi:10.1093/brain/awp209

16.   Bergsland N, Zivadinov R, Schweser F, Hagemeier J, Lichter D, Guttuso T, Jr. Ventral posterior substantia nigra iron increases over 3 years in Parkinson's disease. *Mov Disord*. Jul 2019;34(7):1006-1013. doi:10.1002/mds.27730

17.   Snyder AM, Connor JR. Iron, the substantia nigra and related neurological disorders. *Biochim Biophys Acta*. Jul 2009;1790(7):606-14. doi:10.1016/j.bbagen.2008.08.005

18.   Hughes AJ, Daniel SE, Kilford L, Lees AJ. Accuracy of clinical diagnosis of idiopathic Parkinson's disease: a clinico-pathological study of 100 cases. *J Neurol Neurosurg Psychiatry*. Mar 1992;55(3):181-4. doi:10.1136/jnnp.55.3.181

19.   American Academy of Sleep Medicine. *International classification of sleep disorders*. 2014.

20.   Hoehn MM, Yahr MD. Parkinsonism: onset, progression and mortality. *Neurology*. May 1967;17(5):427-42. doi:10.1212/wnl.17.5.427

21.   Goetz CG, Tilley BC, Shaftman SR, et al. Movement Disorder Society-sponsored revision of the Unified Parkinson's Disease Rating Scale (MDS-UPDRS): scale presentation and clinimetric testing results. *Mov Disord*. Nov 15 2008;23(15):2129-70. doi:10.1002/mds.22340

22.   Mattis S. *Dementia Rating Scale. Professional manual.* Florida: Psychological Assessment Resources; 1988.

23.   Mattis S, Bellak L, Karasu TB. Mental Status Examination for Organic Mental Syndrome in the Elderly Patient. *Geriatric Psychiatry A Handbook for Psychiatrists and Primary Care Physicians*. Grune & Stratton; 1976:chap 77-121.

24.   Nasreddine ZS, Phillips NA, Bedirian V, et al. The Montreal Cognitive Assessment, MoCA: a brief screening tool for mild cognitive impairment. *J Am Geriatr Soc*. Apr 2005;53(4):695-9. doi:10.1111/j.1532-5415.2005.53221.x

25.   Ardouin C, Chereau I, Llorca PM, et al. [Assessment of hyper- and hypodopaminergic behaviors in Parkinson's disease]. *Rev Neurol (Paris)*. Nov 2009;165(11):845-56. Evaluation des troubles comportementaux hyper- et hypodopaminergiques dans la maladie de Parkinson. doi:10.1016/j.neurol.2009.06.003

26.   Rieu I, Martinez-Martin P, Pereira B, et al. International validation of a behavioral scale in Parkinson's disease without dementia. *Mov Disord*. Apr 15 2015;30(5):705-13. doi:10.1002/mds.26223

27.   Marques JP, Kober T, Krueger G, van der Zwaag W, Van de Moortele PF, Gruetter R. MP2RAGE, a self bias-field corrected sequence for improved segmentation and T1-mapping at high field. *Neuroimage*. Jan 15 2010;49(2):1271-81. doi:10.1016/j.neuroimage.2009.10.002

28.   Sasaki M, Shibata E, Tohyama K, et al. Neuromelanin magnetic resonance imaging of locus ceruleus and substantia nigra in Parkinson's disease. *Neuroreport*. Jul 31 2006;17(11):1215-8. doi:10.1097/01.wnr.0000227984.84927.a7

29.   Wang Y, Liu T. Quantitative susceptibility mapping (QSM): Decoding MRI data for a tissue magnetic biomarker. *Magn Reson Med*. Jan 2015;73(1):82-101. doi:10.1002/mrm.25358

30.   Chang L-T. A Method for Attenuation Correction in Radionuclide Computed Tomography. *IEEE Transactions on Nuclear Science*. 1978;25(1):638-643. doi:10.1109/tns.1978.4329385

31.   Santin MD. Optimised Generation of MRI Images by a Multi-Antenna MRI System. 2019;WO2019077246

32.   Liu T, Wisnieff C, Lou M, Chen W, Spincemaille P, Wang Y. Nonlinear formulation of the magnetic field to source relationship for robust quantitative susceptibility mapping. *Magn Reson Med*. Feb 2013;69(2):467-76. doi:10.1002/mrm.24272

33.   Zhou D, Liu T, Spincemaille P, Wang Y. Background field removal by solving the Laplacian boundary value problem. *NMR Biomed*. Mar 2014;27(3):312-9. doi:10.1002/nbm.3064

34.   de Rochefort L, Brown R, Prince MR, Wang Y. Quantitative MR susceptibility mapping using piece-wise constant regularized inversion of the magnetic field. *Magn Reson Med*. Oct 2008;60(4):1003-9. doi:10.1002/mrm.21710

35.   Liu T, Liu J, de Rochefort L, et al. Morphology enabled dipole inversion (MEDI) from a single-angle acquisition: comparison with COSMOS in human brain imaging. *Magn Reson Med*. Sep 2011;66(3):777-83. doi:10.1002/mrm.22816

36.   Liu J, Liu T, de Rochefort L, et al. Morphology enabled dipole inversion for quantitative susceptibility mapping using structural consistency between the magnitude image and the susceptibility map. *Neuroimage*. Feb 1 2012;59(3):2560-8. doi:10.1016/j.neuroimage.2011.08.082

37.   Straub S, Schneider TM, Emmerich J, et al. Suitable reference tissues for quantitative susceptibility mapping of the brain. *Magn Reson Med*. Jul 2017;78(1):204-214. doi:10.1002/mrm.26369

38.   Lim IA, Faria AV, Li X, et al. Human brain atlas for automated region of interest selection in quantitative susceptibility mapping: application to determine iron content in deep gray matter structures. *Neuroimage*. Nov 15 2013;82:449-69. doi:10.1016/j.neuroimage.2013.05.127

39.   Ourselin S, Roche A, Subsol G, Pennec X, Ayache N. Reconstructing a 3D structure from serial histological sections. *Image and Vision Computing*. Jan 2001;19(1-2):25-31. doi:10.1016/s0262-8856(00)00052-4

40.   Modat M, Ridgway GR, Taylor ZA, et al. Fast free-form deformation using graphics processing units. *Comput Methods Programs Biomed*. Jun 2010;98(3):278-84. doi:10.1016/j.cmpb.2009.09.002

41.   Yang J, Huang SC, Mega M, et al. Investigation of partial volume correction methods for brain FDG PET studies. *IEEE Transactions on Nuclear Science*. 1996;43(6):3322-3327. doi:10.1109/23.552745

42.   Patenaude B, Smith SM, Kennedy DN, Jenkinson M. A Bayesian model of shape and appearance for subcortical brain segmentation. *Neuroimage*. Jun 1 2011;56(3):907-22. doi:10.1016/j.neuroimage.2011.02.046

43.   Jenkinson M, Beckmann CF, Behrens TE, Woolrich MW, Smith SM. Fsl. *Neuroimage*. Aug 15 2012;62(2):782-90. doi:10.1016/j.neuroimage.2011.09.015

44.   Gerlach M, Gsell W, Kornhuber J, et al. A post mortem study on neurochemical markers of dopaminergic, GABA-ergic and glutamatergic neurons in basal ganglia-thalamocortical circuits in Parkinson syndrome. *Brain Research*. 1996;741(1-2):142-152. doi:10.1016/s0006-8993(96)00915-8

45.   Tzourio-Mazoyer N, Landeau B, Papathanassiou D, et al. Automated anatomical labeling of activations in SPM using a macroscopic anatomical parcellation of the MNI MRI single-subject brain. *Neuroimage*. Jan 2002;15(1):273-89. doi:10.1006/nimg.2001.0978

46.   O'Brien JT, Colloby S, Fenwick J, et al. Dopamine transporter loss visualized with FP-CIT SPECT in the differential diagnosis of dementia with Lewy bodies. *Arch Neurol*. Jun 2004;61(6):919-25. doi:10.1001/archneur.61.6.919

47.   Bardinet E, Bhattacharjee M, Dormont D, et al. A three-dimensional histological atlas of the human basal ganglia. II. Atlas deformation strategy and evaluation in deep brain stimulation for Parkinson disease. *J Neurosurg*. Feb 2009;110(2):208-19. doi:10.3171/2008.3.17469

48.   Yelnik J, Bardinet E, Dormont D, et al. A three-dimensional, histological and deformable atlas of the human basal ganglia. I. Atlas construction based on immunohistochemical and MRI data. *Neuroimage*. Jan 15 2007;34(2):618-38. doi:10.1016/j.neuroimage.2006.09.026

49.   Haber SN. The place of dopamine in the cortico-basal ganglia circuit. *Neuroscience*. Dec 12 2014;282:248-57. doi:10.1016/j.neuroscience.2014.10.008

50.   *R: A Language and Environment for Statistical Computing*. Version 3.6.1. 2017. https://www.R-project.org/

51.   Prange S, Danaila T, Laurencin C, et al. Age and time course of long-term motor and nonmotor complications in Parkinson disease. *Neurology*. Jan 8 2019;92(2):e148-e160. doi:10.1212/WNL.0000000000006737

52.   Zecca L, Stroppolo A, Gatti A, et al. The role of iron and copper molecules in the neuronal vulnerability of locus coeruleus and substantia nigra during aging. *Proc Natl Acad Sci U S A*. Jun 29 2004;101(26):9843-8. doi:10.1073/pnas.0403495101

53.   Ward RJ, Zucca FA, Duyn JH, Crichton RR, Zecca L. The role of iron in brain ageing and neurodegenerative disorders. *The Lancet Neurology*. 2014;13(10):1045-1060. doi:10.1016/s1474-4422(14)70117-6

54.   Xing Y, Sapuan A, Dineen RA, Auer DP. Life span pigmentation changes of the substantia nigra detected by neuromelanin-sensitive MRI. *Mov Disord*. Nov 2018;33(11):1792-1799. doi:10.1002/mds.27502

55.   van Dyck CH, Seibyl JP, Malison RT, et al. Age-Related Decline in Dopamine Transporters: Analysis of Striatal Subregions, Nonlinear Effects, and Hemispheric Asymmetries. *The American Journal of Geriatric Psychiatry*. 2002;10(1):36-43. doi:10.1097/00019442-200201000-00005

56.   Varrone A, Dickson JC, Tossici-Bolt L, et al. European multicentre database of healthy controls for [123I]FP-CIT SPECT (ENC-DAT): age-related effects, gender differences and evaluation of different methods of analysis. *Eur J Nucl Med Mol Imaging*. Jan 2013;40(2):213-27. doi:10.1007/s00259-012-2276-8

57.   Nichols TE, Holmes AP. Nonparametric permutation tests for functional neuroimaging: a primer with examples. *Hum Brain Mapp*. Jan 2002;15(1):1-25. doi:http://dx.doi.org/10.1002/hbm.1058

58.   Lee CS, Samii A, Sossi V, et al. In vivo positron emission tomographic evidence for compensatory changes in presynaptic dopaminergic nerve terminals in Parkinson's disease. *Annals of Neurology*. 2000;47(4):493-503. doi:10.1002/1531-8249(200004)47:4<493::Aid-ana13>3.0.Co;2-4

59.   Langley J, Huddleston DE, Sedlacik J, Boelmans K, Hu XP. Parkinson's disease-related increase of T2*-weighted hypointensity in substantia nigra pars compacta. *Mov Disord*. Mar 2017;32(3):441-449. doi:10.1002/mds.26883

60.   Pyatigorskaya N, Sanz-Morere CB, Gaurav R, et al. Iron Imaging as a Diagnostic Tool for Parkinson's Disease: A Systematic Review and Meta-Analysis. *Front Neurol*. 2020;11:366. doi:10.3389/fneur.2020.00366

61.   Du G, Liu T, Lewis MM, et al. Quantitative susceptibility mapping of the midbrain in Parkinson's disease. *Mov Disord*. Mar 2016;31(3):317-24. doi:10.1002/mds.26417

62.   Bernheimer H, Birkmayer W, Hornykiewicz O, Jellinger K, Seitelberger F. Brain dopamine and the syndromes of Parkinson and Huntington Clinical, morphological and neurochemical correlations. *Journal of the Neurological Sciences*. 1973;20(4):415-455. doi:10.1016/0022-510x(73)90175-5

63.   Pyatigorskaya N, Gaurav R, Arnaldi D, et al. Magnetic Resonance Imaging Biomarkers to Assess Substantia Nigra Damage in Idiopathic Rapid Eye Movement Sleep Behavior Disorder. *Sleep*. Nov 1 2017;40(11)doi:10.1093/sleep/zsx149

64.   Sun J, Lai Z, Ma J, et al. Quantitative evaluation of iron content in idiopathic rapid eye movement sleep behavior disorder. *Mov Disord*. Mar 2020;35(3):478-485. doi:10.1002/mds.27929

65.   Gaurav R, Yahia-Cherif L, Pyatigorskaya N, et al. Longitudinal changes in Neuromelanin MRI Signal in Parkinson's Disease: A progression marker. Movement Disorders (in press)2021.

66.   Sulzer D, Cassidy C, Horga G, et al. Neuromelanin detection by magnetic resonance imaging (MRI) and its promise as a biomarker for Parkinson's disease. *NPJ Parkinsons Dis*. 2018;4:11. doi:10.1038/s41531-018-0047-3

67.   McGeer PL, Itagaki S, Boyes BE, McGeer EG. Reactive microglia are positive for HLA-DR in the substantia nigra of Parkinson's and Alzheimer's disease brains. *Neurology*. Aug 1988;38(8):1285-91. doi:10.1212/wnl.38.8.1285

68.   Beach TG, Sue LI, Walker DG, et al. Marked microglial reaction in normal aging human substantia nigra: correlation with extraneuronal neuromelanin pigment deposits. *Acta Neuropathol*. Oct 2007;114(4):419-24. doi:10.1007/s00401-007-0250-5

69.   Carballo-Carbajal I, Laguna A, Romero-Gimenez J, et al. Brain tyrosinase overexpression implicates age-dependent neuromelanin production in Parkinson's disease pathogenesis. *Nat Commun*. Mar 7 2019;10(1):973. doi:10.1038/s41467-019-08858-y

70.   Kraemmer J, Kovacs GG, Perju-Dumbrava L, Pirker S, Traub-Weidinger T, Pirker W. Correlation of striatal dopamine transporter imaging with post mortem substantia nigra cell counts. *Mov Disord*. Dec 2014;29(14):1767-73. doi:10.1002/mds.25975

71.   Karimi M, Tian L, Brown CA, et al. Validation of nigrostriatal positron emission tomography measures: critical limits. *Ann Neurol*. Mar 2013;73(3):390-6. doi:10.1002/ana.23798

72.   Bronfeld M, Bar-Gad I. Loss of specificity in Basal Ganglia related movement disorders. *Front Syst Neurosci*. 2011;5:38. doi:10.3389/fnsys.2011.00038

73.   Postuma RB, Iranzo A, Hu M, et al. Risk and predictors of dementia and parkinsonism in idiopathic REM sleep behaviour disorder: a multicentre study. *Brain*. Mar 1 2019;142(3):744-759. doi:10.1093/brain/awz030

74.   Fereshtehnejad SM, Yao C, Pelletier A, Montplaisir JY, Gagnon JF, Postuma RB. Evolution of prodromal Parkinson's disease and dementia with Lewy bodies: a prospective study. *Brain*. Jul 1 2019;142(7):2051-2067. doi:10.1093/brain/awz111

75.   Dusek P, Ibarburu V, Bezdicek O, et al. Relations of non-motor symptoms and dopamine transporter binding in REM sleep behavior disorder. *Sci Rep*. Oct 29 2019;9(1):15463. doi:10.1038/s41598-019-51710-y

76.   Iranzo A, Santamaria J, Valldeoriola F, et al. Dopamine transporter imaging deficit predicts early transition to synucleinopathy in idiopathic rapid eye movement sleep behavior disorder. *Ann Neurol*. Sep 2017;82(3):419-428. doi:10.1002/ana.25026

77.   Knudsen K, Fedorova TD, Hansen AK, et al. In-vivo staging of pathology in REM sleep behaviour disorder: a multimodality imaging case-control study. *The Lancet Neurology*. 2018;17(7):618-628. doi:10.1016/s1474-4422(18)30162-5

78.   Stokholm MG, Iranzo A, Østergaard K, et al. Assessment of neuroinflammation in patients with idiopathic rapid-eye-movement sleep behaviour disorder: a case-control study. *The Lancet Neurology*. 2017;16(10):789-796. doi:10.1016/s1474-4422(17)30173-4

79.   Coakeley S, Cho SS, Koshimori Y, et al. [(18)F]AV-1451 binding to neuromelanin in the substantia nigra in PD and PSP. *Brain Struct Funct*. Mar 2018;223(2):589-595. doi:10.1007/s00429-017-1507-y

80.   Stoessl AJ. Central pharmacokinetics of levodopa: Lessons from imaging studies. *Mov Disord*. Jan 2015;30(1):73-9. doi:10.1002/mds.26046

Figure legends

Figure 1 Group differences in striatal DaT levels. Functional subregions in the striatum **(A)**. The panels on the left-hand and right-hand sides respectively show the results of the statistical comparison between groups in the clinically most and least affected brain hemispheres. Each panel has three columns, representing the inter-group comparison between Parkinson's disease patients and HCs (left), Parkinson's disease patients and iRBD patients (centre) or iRBD patients and HCs (right). The three rows correspond to the group differences at V1 **(B-G)**, the group differences at V2 **(H-M)**, and the inter-visit differences in longitudinal subjects **(N-S)**. Results were adjusted for age and sex and corrected for multiple comparisons using Tukey's test at the $P < 0.05$ level. For improved clarity in the visual

representation of statistical differences, p-values were converted into z-scores. V1/V2 = visit one or two; HCs = healthy control subjects; iRBDs = iRBD patients; PDs = Parkinson's disease patients; Cd = caudate nucleus; NAc = nucleus accumbens; Pu = putamen.

Figure 2 Group differences in nigral neuromelanin and nigral iron levels. Functional subregions in the substantia nigra **(A)**. The panels on the left-hand and right-hand sides respectively show the results of the statistical comparison between groups in the clinically most and least affected brain hemispheres. The two rows correspond to the group differences at V1 **(B-E)**, and the group differences at V2 **(F-I)**. Nonsignificant between-group comparisons were omitted. Results were adjusted for age and sex and corrected for multiple comparisons using Tukey's test at the $P < 0.05$ level. For improved clarity in the visual representation of statistical differences, p-values were converted into z-scores. V1/V2 = visit one or two; HCs = healthy control subjects; iRBDs = iRBD patients; PDs = Parkinson's disease patients; NM = neuromelanin.

Figure 3 Temporal changes in striatal DaT, nigral neuromelanin and nigral iron in patients relative to healthy controls. For all Parkinson's disease patients relative to HCs, in each striatal region and each brain hemisphere, the figure shows the mono-exponential functions fitting the regional DaT-SBR percent change against disease duration **(A-C, F-H)**. For each nigral region in the most affected hemisphere, the figure also shows the mono-exponential functions fitting iron (QSM) or neuromelanin (NM SNR) percent changes against disease duration **(D, E)**. Cd = caudate nucleus; NAc = nucleus accumbens; NM = neuromelanin; Pu = putamen; SBR = specific binding ratio; iRBDs = iRBD patients; PDs = Parkinson's disease patients; QSM = quantitative susceptibility mapping; SNR = signal-to-noise ratio; V1/V2 = visit one or two.

Figure 4 Spatial correlation patterns between nigral neuromelanin or nigral iron and striatal DaT in the SNc. For each striatal region (putamen, caudate nucleus and nucleus accumbens) and each functional territory (sensorimotor, associative and limbic), the DaT-neuromelanin correlation patterns **(A-G)**, the neuromelanin-iron correlation patterns **(K)** and the DaT-iron correlation patterns **(L-R)** in the SNc are shown overlaid on the brain template. The DaT-neuromelanin regional overlaps are shown for the putamen, caudate and limbic areas **(H-J)** along with Dice scores quantifying the relative overlap between pairs of correlation patterns. In each image, the brain template is displayed using the same intensity range in arbitrary units. All images are displayed showing the most affected brain hemisphere

on the left side of the image. For improved image visualisation quality, the correlation patterns **(A-G, K, L-R)** were spatially upsampled by a factor of four using nearest-neighbour interpolation. AS = associative; Cd = caudate nucleus; iRBDs = iRBD patients; LI = limbic; NAc = nucleus accumbens; PDs = Parkinson's disease patients; Pu = putamen; SM = sensorimotor.
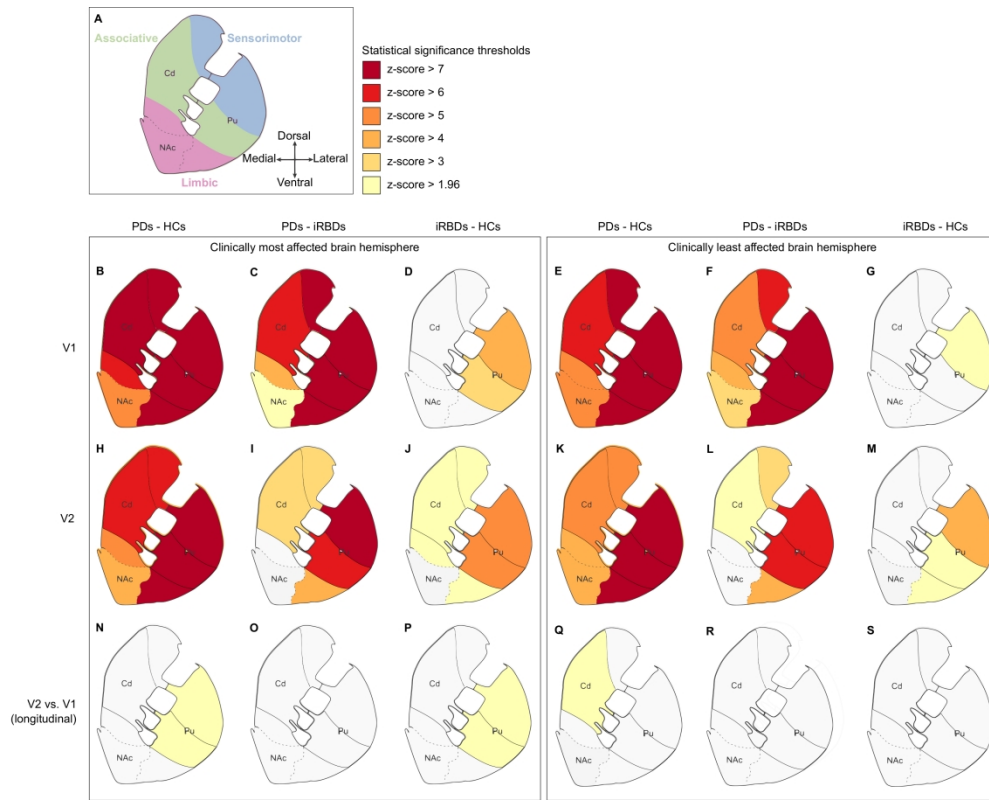
Figure 1

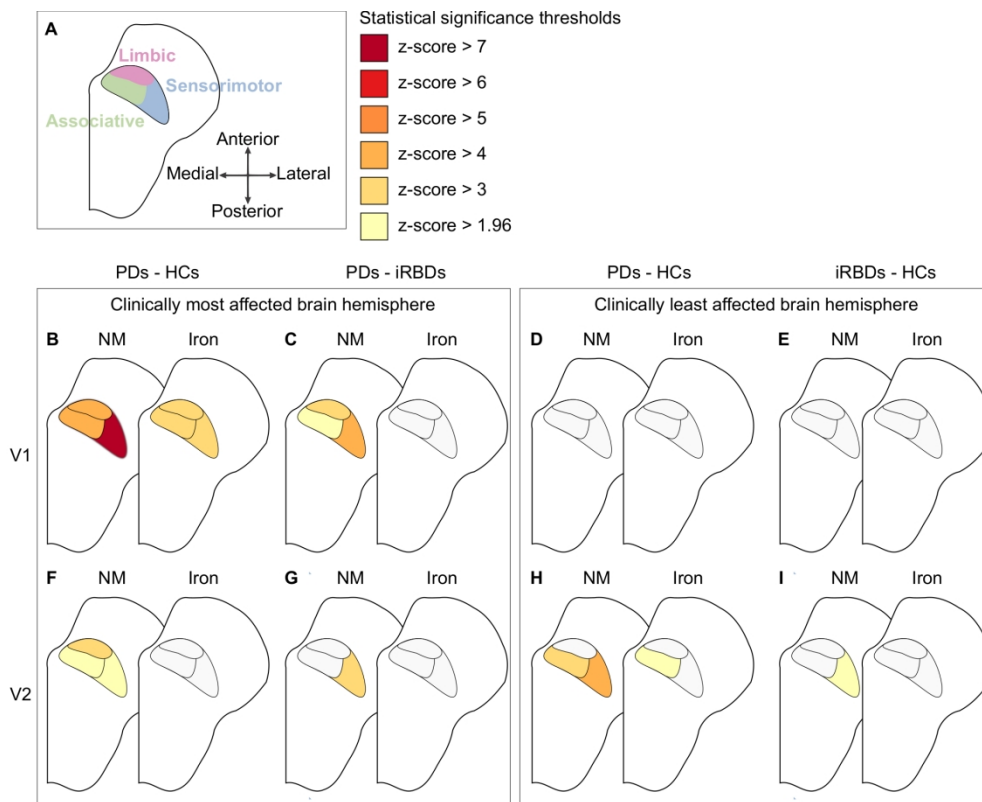278x220mm (300 x 300 DPI)
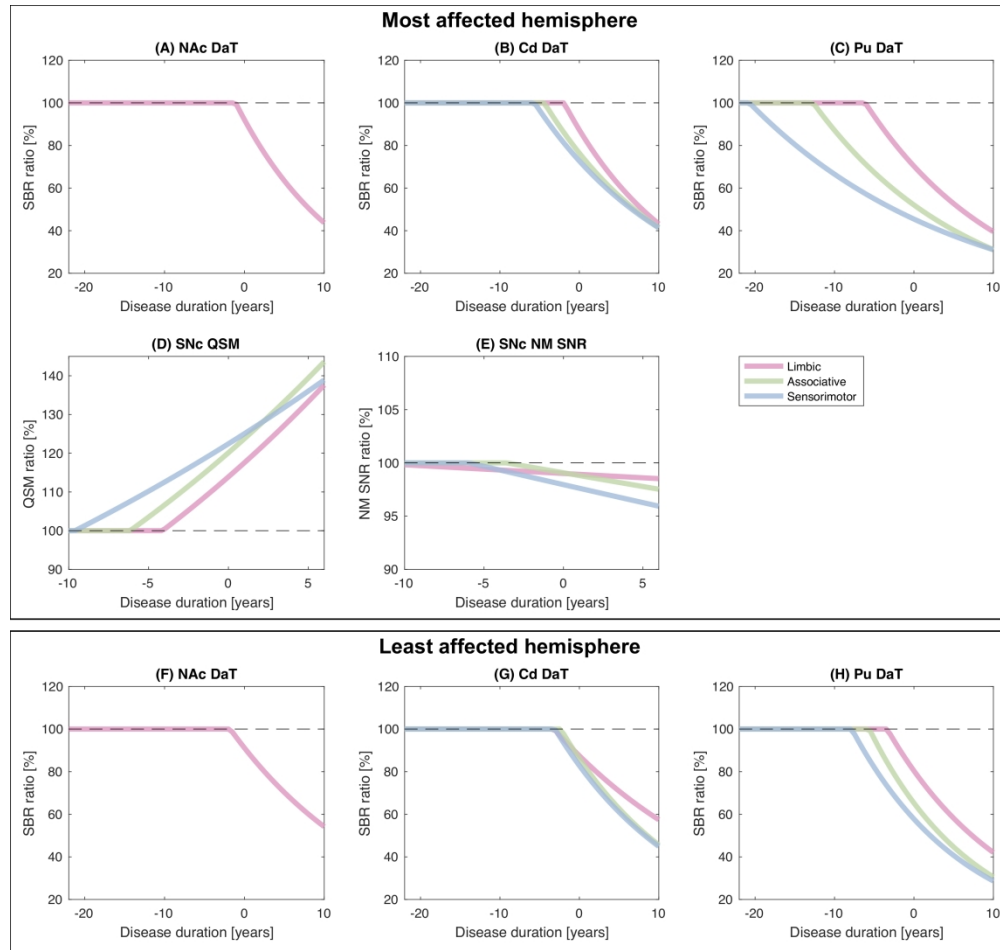
Figure 2

179x142mm (300 x 300 DPI)

Figure 3

272x257mm (300 x 300 DPI)
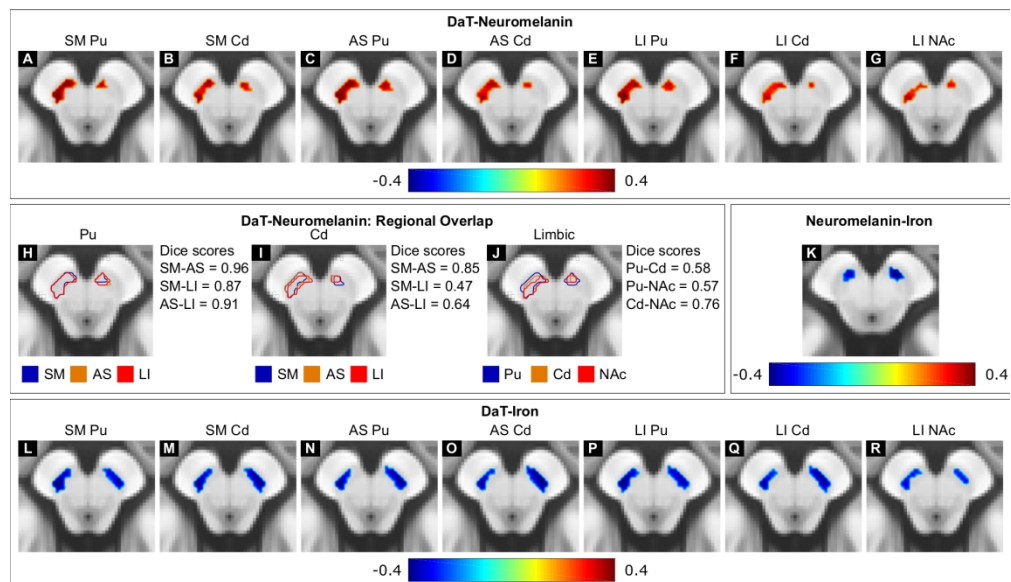
Figure 4

174x100mm (300 x 300 DPI)

Table 1 Demographic and clinical characteristics of the cohort

	HCs		iRBDs		PDs	
	V1	V2	V1	V2	V1	V2
Number of subjects	55	28	43	21	135	83
Age (years)	62.0 ± 9.2	62.3 ± 8.9	67.6 ± 5.1*	69.2 ± 5.3	61.6 ± 9.4#	63.9 ± 9.1
Sex (M/F)	30/25	9/19	38/5*	17/4	85/50#	52/31
Time from V1 (years)	n/a	2.0 ± 0.1	n/a	2.1 ± 0.2	n/a	1.9 ± 0.4
Disease duration (years)	n/a	n/a	n/a	1.1 ± 0.5 [4 iRBDs]	1.5 ± 1.1	3.7 ± 1.1
Hoehn & Yahr stage	0.1 ± 0.5	0.1 ± 0.4	0.7 ± 1.0*	1.2 ± 0.9	2.0 ± 0.2 *#	2.0 ± 0.2
LEDD (mg)	n/a	n/a	n/a	210.5 ± 181.7 [4 iRBDs]	350.6 ± 252.6 [121 PDs]	490.8 ± 267.5 [77 PDs]
MDS-UPDRS III OFF	5.5 ± 5.2	6.8 ± 5.4	11.5 ± 6.3*	19.0 ± 8.3	30.3 ± 7.8 *,#	33.9 ± 7.8
MoCA	28.0 ± 1.7	28.6 ± 1.8	27.3 ± 2.3	26.7 ± 3.2	27.4 ± 2.2	27.2 ± 3.6
MATTIS DRS	139.6 ± 3.9	141.3 ± 3.0	137.3 ± 6.2*	139.5 ± 4.5	138.9 ± 4.4	136.7 ± 15.8
ASBPD hypodopaminergic	0.8 ± 1.0	0.7 ± 1.2	1.7 ± 2.5	2.4 ± 3.1	2.0 ± 1.9*	2.1 ± 1.9
ASBPD hyperdopaminergic	0.1 ± 0.4	0.2 ± 0.5	0.3 ± 0.7	0.4 ± 1.0	1.1 ± 1.5*,#	1.3 ± 1.8
Laterality of first motor symptoms in the body (right/left)	n/a	n/a	n/a	n/a	78/57	46/37
DaTScan™ delay relative to MRI (years)	0.2 ± 0.2	0.2 ± 0.3	0.3 ± 0.2	0.1 ± 0.1	0.2 ± 0.2	0.1 ± 0.2

Values are means ± standard deviations

*$P < 0.05$ denote significant differences between PDs or iRBDs and HCs at V1

#$P < 0.05$ denote significant differences between PDs and iRBDs at V1

n/a = not available

V1/V2 = visit one or two; HCs = healthy control subjects; iRBDs = iRBD patients; PDs = Parkinson's disease patients; LEDD = Levodopa equivalent daily dose; MDS-UPDRS = Movement Disorder Society unified Parkinson's disease rating scale; MoCA = Montréal cognitive assessment score; MATTIS DRS = Mattis' dementia rating scale; ASBPD = Ardouin's scale for behavior in PD